ALMA Memo 318
Amplitude Calibration at Millimeter and Submillimeter Wavelengths

Jeffrey G. Mangum
National Radio Astronomy Observatory Tucson
email: jmangum@nrao.edu

August 9, 2000

Abstract

Accurate amplitude calibration at millimeter and submillimeter wavelengths is a difficult goal to achieve due to the temporal variability of the emissive and absorptive properties of the Earth's atmosphere and the lack of an accurate astronomical flux standard. The difficulties with deriving a uniform amplitude calibration system has resulted in the three step calibration process used at millimeter and submillimeter single dishes and interferometers. The second step in this process involves the *chopper wheel calibration technique*. Chopper wheel calibration is used to derive the antenna temperature of an astronomical source corrected for atmospheric extinction. An analysis of the uncertainties in two variants of this technique, one which uses a single calibrated load and a second which uses two calibrated loads, has been derived. The conclusion of this analysis is that the one-load chopper calibration system is more uncertain than the two-load chopper calibration system for application at submillimeter wavelengths. The main reason for the larger uncertainty of the one-load chopper calibration system is the fact that it requires a knowledge of the mean atmospheric temperature, which is inherently difficult to obtain. Of the two calibration systems, the two-load chopper system has the potential for reaching a calibration accuracy of approximately 1% for all bands, as specified for the ALMA receiving systems. We will also address the problem of deriving the third and final step on the amplitude

calibration ladder; the conversion of atmosphere-corrected antenna temperatures (T_A^*) to astronomical source radiation temperatures.

To place this discussion in the context of general temperature scales used in millimeter and submillimeter astronomy, a discussion of temperature scales and telescope efficiencies is given in an appendix of this paper.

1 Introduction

Over the last 30 years considerable effort has been devoted to the development of an absolute calibration technique for millimeter astronomical measurements. The three most significant problems which one must overcome when calibrating the amplitude of millimeter astronomical measurements are:

- Implementation of a stable total power system;
- The variable attenuation of millimeter signals due to the Earth's atmosphere. This opacity is due primarily to the combined absorptive and emissive effects of O_2 and H_2O;
- The lack of an appropriate astronomical amplitude calibration source.

In the following, we describe the amplitude calibration scheme used at millimeter and submillimeter wavelengths and address the needs for accurate amplitude calibration for ALMA. In this analysis, we consider most sources of uncertainty **except** uncertainty due to:

- pointing errors,
- variations in the antenna beam pattern with time and elevation,
- loss of correlation due to atmospheric or instrumental phase noise,
- gain compression in the SIS mixer or amplifiers, and
- variations in the coupling of the receiver beams to the calibration loads.

2 The Millimeter and Submillimeter Amplitude Calibration Ladder

A graphical description of the "calibration ladder" used at millimeter and submillimeter wavelengths is shown in Figure 1. The uncertainties associated with each step of the ladder are typical of the current calibration systems used at existing millimeter wavelength observatories. The target uncertainties for amplitude calibration with ALMA are listed in parentheses for each step. In the following sections, we will address the techniques used to define each step of the calibration ladder, and will define the uncertainties associated with each.

3 The First Step: Accurate Total Power Measurement

The first step of the amplitude calibration ladder is the easiest of the three steps to derive. Good gain stability, to a level of at least 1% over time scales less than approximately 10 seconds, are relatively easy to maintain with well-built receiving systems. The gain stability specification for ALMA is 10^{-4} over time scales $\leq$1 second.

4 The Second Step: Calculation of the $\mathbf{T_A^*}$ Temperature Scale

Calibration of the telescope-dependent amplitude scale for most astronomical measurements is accomplished through the measurement of a noise source of known emissive properties. At centimeter wavelengths the common noise source used for calibration is a waveguide oscillator or diode which emits a broadband noise source directly into the radio receiver. At shorter wavelengths, noise tube or diode calibration sources become problematic to use due to their frequency-, time-, and polarization-dependent output characteristics. The difficulties encountered in applying noise tube calibration to millimeter astronomical measurements lead Penzias & Burrus (1973) to develop the chopper wheel calibration technique. In this technique, the response of the receiver is calibrated by alternately introducing and removing black body

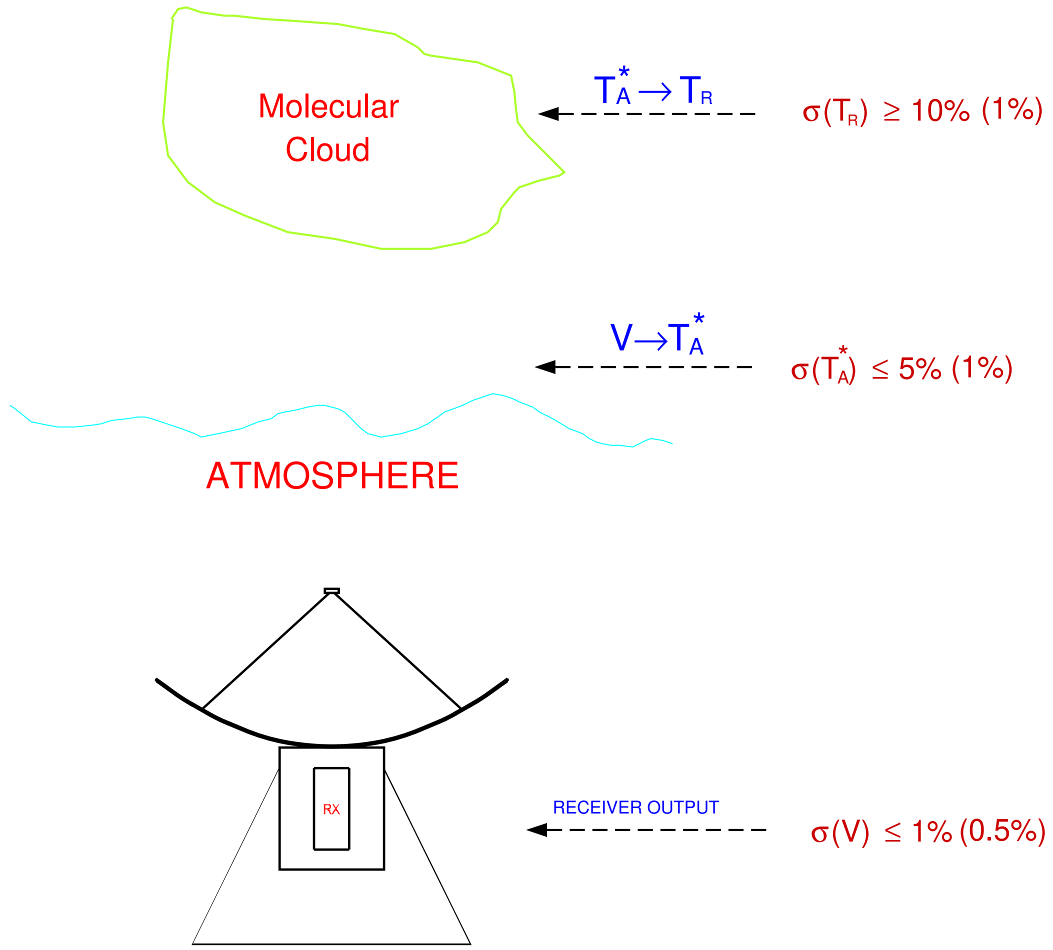

Figure 1: Graphical representation of the "calibration ladder" used at millimeter and submillimeter wavelengths. The current state of the art for determining each step of the ladder is indicated, along with the ALMA requirements for each in parentheses. The chopper wheel calibration technique is used to determine the second step in this ladder.

absorbers of known or estimated physical temperature at a convenient point in the signal path of the receiver. The calibrating noise signal is then the difference between the temperatures of these absorbers. The broad band and frequency independent emissive properties of the absorbers, coupled with the simplicity and reliability of this technique, has resulted in its adoption as the main calibration system used at most radio observatories which operate at millimeter wavelengths.

The chopper wheel calibration technique represents the second step in the "calibration ladder" (Figure 1), which is the conversion of measured voltages at the receiver to an antenna temperature corrected for the time- and position-variable emissive properties of the Earth's atmosphere. In the following, we investigate the accuracy of two forms of the chopper wheel calibration technique when applied to observations at millimeter and sub-millimeter wavelengths. Definitions for the terms used in this analysis can be found in Appendix A.

4.1 Terms Used in the $\mathbf{T_A^*}$ Temperature Scale

The received signals from the sky, load, and source measurements are given by

$$
\begin{aligned}
V_{sky} &= K\big[G_s J(\nu_s, T_A(sky)) + G_i J(\nu_i, T_A(sky)) + T_{rx}\big] + V_{offset} \\
&= K\{G_s\big[J(\nu_s, T_{sky}^{cold}) + J(\nu_s, T_{sky}^{hot}) + J(\nu_s, T_{ant}) + J(\nu_s, T_{bg})\big] + \\
&\quad G_i\big[J(\nu_i, T_{sky}^{cold}) + J(\nu_i, T_{sky}^{hot}) + J(\nu_i, T_{ant}) + J(\nu_i, T_{bg})\big] + \\
&\quad T_{rx}\} + V_{offset} \\
&= K\big[G_s\{\eta_l J(\nu_s, T_m)\big[1 - \exp(-\tau_s)\big] + (1-\eta_l) J(\nu_s, T_{spill}) + \\
&\quad \eta_l J(\nu_s, T_{bg}) \exp(-\tau_s)\} + \\
&\quad G_i\{\eta_l J(\nu_i, T_m)\big[1 - \exp(-\tau_i)\big] + (1-\eta_l) J(\nu_i, T_{spill}) + \\
&\quad \eta_l J(\nu_i, T_{bg}) \exp(-\tau_i)\} + T_{rx}\big] + V_{offset} \qquad (1)
\end{aligned}
$$

$$
V_{load} = K\left[G_s J(\nu_s, T_{load}) + G_i J(\nu_i, T_{load}) + T_{rx}\right] + V_{offset} \qquad (2)
$$

$$
\begin{aligned}
V_{source} &= K\big[G_s J(\nu_s, T_A(sky)) + G_i J(\nu_i, T_A(sky)) + \\
&\quad T_A(source) + T_{rx}\big] + V_{offset} \\
&= K\Bigg[G_s J(\nu_s, T_A(sky)) + G_i J(\nu_i, T_A(sky)) + \\
&\quad \eta_l\left[T^*_{As} G_s \exp(-\tau_s) + T^*_{Ai} G_i \exp(-\tau_i)\right] + T_{rx}\Bigg] + V_{offset}
\end{aligned} \tag{3}
$$

Note that Equation 1 is equivalent to Equation 3 in Ulich & Haas (1976). Using the definitions for V_{sky} (Equation 1), V_{load} (Equation 2), and V_{source} (Equation 3), and noting that

$$
V_{source} - V_{sky} = K\eta_l\left[T^*_{As} G_s \exp(-\tau_s) + T^*_{Ai} G_i \exp(-\tau_i)\right] \tag{4}
$$

we can assume that the signal to be observed exists only in the signal sideband (so that $T^*_{As} = T^*_A$) to derive the standard equation for T^*_A

$$
\boxed{T^*_A = \frac{V_{source} - V_{sky}}{K G_s \eta_l \exp(-\tau_s)}} \tag{5}
$$

A common calibration factor used to quantify millimeter and submillimeter measurements acquired with both single dish and interferometric techniques is the system temperature T_{sys}, which is defined as

$$
T_{sys} \equiv \frac{V_{sky}}{V_{source} - V_{sky}}\left(T^*_{As} + T^*_{Ai}\right) \tag{6}
$$

Using Equations 1, 3, and 5, Equation 6 becomes

$$
T_{sys} = \frac{G_s J(\nu_s, T_A(sky)) + G_i J(\nu_i, T_A(sky)) + T_{rx}}{\eta_l\left[T^*_{As} G_s \exp(-\tau_s) + T^*_{Ai} G_i \exp(-\tau_i)\right]}\left[T^*_{As} + T^*_{Ai}\right] \tag{7}
$$

If we are only interested in signals which come from the signal sideband, then $T^*_{Ai} = 0$. Therefore, with $T^*_{As} = T^*_A$, Equation 7 becomes

$$\boxed{T_{sys} = \frac{J(\nu_s, T_A(sky)) + T_{rx}}{G_s \eta_l \exp(-\tau_s)}} \tag{8}$$

Note that Equation 8 requires a measurement of T_{rx}, which is derived from sequential measurements of two calibrated loads at known temperatures $T_{load,1}$ and $T_{load,2}$

$$\begin{aligned} T_{rx} &= \frac{T_{load,1}V_{load,2} - T_{load,2}V_{load,1}}{V_{load,1} - V_{load,2}} \\ &= \frac{T_{load,1} - YT_{load,2}}{Y - 1} \end{aligned} \tag{9}$$

where $Y \equiv \frac{V_{load,1}}{V_{load,2}}$.

4.2 Derivation and Calibration of the T_A^* Temperature Scale

Proper scaling of the T_A^* and T_{sys} temperatures in millimeter and submillimeter single dish and interferometric observations requires the measurement of calibrated loads. The traditional mode for deriving and calibrating the T_A^* and T_{sys} temperature scales at millimeter wavelengths is the "chopper wheel" technique (Penzias & Burrus 1973; Ulich & Haas 1976). In the chopper wheel calibration system, the response of the receiver to one or two calibrated loads is combined with a measurement of the emission due to the sky to derive T_A^* and T_{sys}. In both flavours of the chopper wheel calibration technique, it is assumed that G_s and η_l are known. In the following, we will discuss the two main variants of the chopper wheel calibration technique.

4.2.1 Two–Load Chopper Wheel

The most direct way to measure T_A^* and T_{sys} is to use the two–load chopper wheel calibration technique. As one can see by examining Equations 5, 8, and 9, two calibrated loads are required to directly measure K in Equation 5, and $T_A(sky)$ and T_{rx} in Equation 8. We will derive each of these in the following.

1. A direct measure of K is derived by noting that

$$
\begin{aligned}
T_{load,1} &= \frac{(V_{load,1} + V_{offset})}{K} && (10)\\
T_{load,2} &= \frac{(V_{load,2} + V_{offset})}{K} && (11)
\end{aligned}
$$

   Taking the difference of these two equations and solving for K yields

$$K = \frac{V_{load,1} - V_{load,2}}{T_{load,1} - T_{load,2}} \tag{12}$$

   so that

$$\boxed{T_A^* = \left(\frac{T_{load,1} - T_{load,2}}{V_{load,1} - V_{load,2}}\right) \frac{V_{source} - V_{sky}}{G_s \eta_l \exp(-\tau_s)}} \tag{13}$$

2. The unknown quantity $T_A(sky)$ in Equation 8 can be derived by noting that

$$
\begin{aligned}
K &= \frac{V_{load,1} - V_{sky}}{T_{load,1} - T_A(sky) - T_{rx}} && (14)\\
&= \frac{V_{load,2} - V_{sky}}{T_{load,2} - T_A(sky) - T_{rx}} && (15)
\end{aligned}
$$

   Equating these two relations for K and solving for $T_A(sky)$ yields

$$
\begin{aligned}
T_A(sky) &= \frac{V_{sky}}{K}\\
&= \frac{(V_{load,1} - V_{sky})\, T_{load,2} - (V_{load,2} - V_{sky})\, T_{load,1}}{V_{load,1} - V_{load,2}} - T_{rx} && (16)
\end{aligned}
$$

3. T_{rx} is gotten from Equation 9.

The main shortcoming of the two-load chopper wheel technique is that a measurement of the atmospheric opacity in the signal sideband at the elevation of the source, τ_s, is required. This measurement is currently gotten by making a tipping scan in the direction of the source.

4.2.2 One–Load Chopper Wheel (Traditional Chopper Wheel)

The one-load chopper wheel technique is the simplest to implement as it requires only a chopping vane placed over the feed of the receiver. Its main shortcoming is that a model of the emission due to the sky must be used to derive T_A^* and T_{sys}. In the following, we will derive the dependence of T_A^* on the various measurable terms in a one-load chopper wheel system.

Starting with Equation 5 and a difference between a total power measurement of the load and the sky given by

$$\begin{aligned}
\Delta V_{cal} &= V_{load} - V_{sky} \\
&= K\Big[G_s J(\nu_s, T_{load}) + G_i J(\nu_i, T_{load}) + T_{rx} - \\
&\quad G_s\{\eta_l J(\nu_s, T_m)\left[1 - \exp(-\tau_s)\right] + (1-\eta_l) J(\nu_s, T_{spill}) + \\
&\quad \eta_l J(\nu_s, T_{bg}) \exp(-\tau_s)\} - \\
&\quad G_i\{\eta_l J(\nu_i, T_m)\left[1 - \exp(-\tau_i)\right] + (1-\eta_l) J(\nu_i, T_{spill}) + \\
&\quad \eta_l J(\nu_i, T_{bg}) \exp(-\tau_i)\} - T_{rx}\Big] \qquad (17)
\end{aligned}$$

we can solve for K in Equation 17 and substitute it into Equation 5 to yield the following relation for T_A^*

$$\begin{aligned}
T_A^* &= \frac{V_{source} - V_{sky}}{V_{load} - V_{sky}} \left\{ \frac{1}{G_s \eta_l \exp(-\tau_s)} \right\} \\
&\quad \Big[G_s J(\nu_s, T_{load}) + G_i J(\nu_i, T_{load}) + T_{rx} - \\
&\quad G_s\{\eta_l J(\nu_s, T_m)\left[1 - \exp(-\tau_s)\right] + (1-\eta_l) J(\nu_s, T_{spill}) + \\
&\quad \eta_l J(\nu_s, T_{bg}) \exp(-\tau_s)\} - \\
&\quad G_i\{\eta_l J(\nu_i, T_m)\left[1 - \exp(-\tau_i)\right] + (1-\eta_l) J(\nu_i, T_{spill}) + \\
&\quad \eta_l J(\nu_i, T_{bg}) \exp(-\tau_i)\} - T_{rx}\Big] \qquad (18)
\end{aligned}$$

which, following rearrangement, yields

$$
\boxed{\begin{aligned}
T_A^* =& \frac{V_{source} - V_{sky}}{V_{load} - V_{sky}} \\
& \Bigg\{ J(\nu_s, T_m) - J(\nu_s, T_{bg}) + \\
& \Big\{ J(\nu_s, T_{load}) - J(\nu_s, T_{spill}) + R_i \big[J(\nu_i, T_{load}) - J(\nu_i, T_{spill}) \big] \Big\} \frac{\exp(\tau_s)}{\eta_l} + \\
& \Big\{ J(\nu_s, T_{spill}) - J(\nu_s, T_m) + R_i \big[J(\nu_i, T_{spill}) - J(\nu_i, T_m) \big] \Big\} \exp(\tau_s) + \\
& R_i \big[J(\nu_i, T_m) - J(\nu_i, T_{bg}) \big] \exp(\tau_s - \tau_i) \Bigg\}
\end{aligned}} \tag{19}
$$

Note that for $T_m \simeq T_{spill} \simeq T_{load}$ and $\tau_s \simeq \tau_i$, Equation 19 is independent of τ.

A common quantity used at millimeter and submillimeter observatories which use the one-load chopper wheel technique is the "calibration temperature" T_c. In Equation 19 T_c is given by

$$
\begin{aligned}
T_c \quad = \quad & \Bigg\{ J(\nu_s, T_m) - J(\nu_s, T_{bg}) + \\
& \Big\{ J(\nu_s, T_{load}) - J(\nu_s, T_{spill}) + R_i \big[J(\nu_i, T_{load}) - J(\nu_i, T_{spill}) \big] \Big\} \frac{\exp(\tau_s)}{\eta_l} + \\
& \Big\{ J(\nu_s, T_{spill}) - J(\nu_s, T_m) + R_i \big[J(\nu_i, T_{spill}) - J(\nu_i, T_m) \big] \Big\} \exp(\tau_s) + \\
& R_i \Bigg[J(\nu_i, T_m) - J(\nu_i, T_{bg}) \Bigg] \exp(\tau_s - \tau_i) \Bigg\}
\end{aligned} \tag{20}
$$

4.3 Variance of the $\mathbf{T_A^*}$ Scale

4.3.1 Two-Load Chopper Wheel

In the following, we assume that $V_{load,1}$, $V_{load,2}$, V_{source}, and V_{sky} can be measured exactly. We can now calculate the variance of T_A^* with respect to the free variables $T_{load,1}$, $T_{load,2}$, G_s, η_l, and τ_s

$$
\begin{aligned}
\sigma^2(T_A^*)^{two-load} &= \sigma^2(T_{load,1})\left(\frac{\partial T_A^*}{\partial T_{load,1}}\right)^2 + \sigma^2(T_{load,2})\left(\frac{\partial T_A^*}{\partial T_{load,2}}\right)^2 + \\
&\quad \sigma^2(G_s)\left(\frac{\partial T_A^*}{\partial G_s}\right)^2 + \sigma^2(\eta_l)\left(\frac{\partial T_A^*}{\partial \eta_l}\right)^2 + \\
&\quad \sigma^2(\tau_s)\left(\frac{\partial T_A^*}{\partial \tau_s}\right)^2 \qquad (21)
\end{aligned}
$$

Calculating the partial derivatives of Equation 13

$$
\begin{aligned}
\frac{\partial T_A^*}{\partial T_{load,1}} &= \left(\frac{1}{V_{load,1}-V_{load,2}}\right)\frac{V_{source}-V_{sky}}{G_s\eta_l\exp(-\tau_s)} && (22)\\
&= \frac{T_A^*}{T_{load,1}-T_{load,2}} && (23)\\
\frac{\partial T_A^*}{\partial T_{load,2}} &= -\left(\frac{1}{V_{load,1}-V_{load,2}}\right)\frac{V_{source}-V_{sky}}{G_s\eta_l\exp(-\tau_s)} && (24)\\
&= -\frac{T_A^*}{T_{load,1}-T_{load,2}} && (25)\\
\frac{\partial T_A^*}{\partial \eta_l} &= -\left(\frac{V_{load,1}-V_{load,2}}{T_{load,1}-T_{load,2}}\right)\frac{V_{source}-V_{sky}}{G_s\eta_l^2\exp(-\tau_s)} && (26)\\
&= -\frac{T_A^*}{\eta_l} && (27)\\
\frac{\partial T_A^*}{\partial \tau_s} &= \left(\frac{V_{load,1}-V_{load,2}}{T_{load,1}-T_{load,2}}\right)\frac{V_{source}-V_{sky}}{G_s\eta_l\exp(-\tau_s)} && (28)\\
&= T_A^* && (29)\\
\frac{\partial T_A^*}{\partial G_s} &= -\left(\frac{V_{load,1}-V_{load,2}}{T_{load,1}-T_{load,2}}\right)\frac{V_{source}-V_{sky}}{G_s^2\eta_l\exp(-\tau_s)} && (30)\\
&= -\frac{T_A^*}{G_s} && (31)
\end{aligned}
$$

Substituting the partial derivatives into our variance equation leads to the following equation for the variance of T_A^* in the two-load chopper wheel technique

$$\sigma^2(T_A^*)^{two-load} = \sigma^2(T_{load,1})\left(\frac{T_A^*}{T_{load,1}-T_{load,2}}\right)^2 + \sigma^2(T_{load,2})\left(\frac{T_A^*}{T_{load,1}-T_{load,2}}\right)^2 + \sigma^2(G_s)\left(\frac{T_A^*}{G_s}\right)^2 + \sigma^2(\eta_l)\left(\frac{T_A^*}{\eta_l}\right)^2 + \sigma^2(\tau_s)\,(T_A^*)^2 \quad (32)$$

and the full variance relation for T_A^* using the two-load chopper wheel technique

$$\left(\frac{\sigma(T_A^*)}{T_A^*}\right)^{two-load} = \sqrt{\frac{\sigma^2(T_{load,1})+\sigma^2(T_{load,2})}{(T_{load,1}-T_{load,2})^2} + \frac{\sigma^2(G_s)}{G_s^2} + \frac{\sigma^2(\eta_l)}{\eta_l^2} + \sigma^2(\tau_s)} \quad (33)$$

To get an order-of-magnitude estimate of $\frac{\sigma(T_A^*)}{T_A^*}$, we assume $\eta_l \simeq 1$. Doing this with Equation 33 we get the following

$$\mathcal{O}\left(\frac{\sigma(T_A^*)}{T_A^*}\right)^{two-load} = \sqrt{\mathcal{O}\left(\frac{\sigma^2(T_{load,1})+\sigma^2(T_{load,2})}{(T_{load,1}-T_{load,2})^2}\right) + \mathcal{O}\left(\frac{\sigma^2(G_s)}{G_s^2}\right) + \mathcal{O}\left(\sigma^2(\eta_l)\right) + \mathcal{O}\left(\sigma^2(\tau_s)\right)} \quad (34)$$

4.3.2 One-Load Chopper Wheel

In the following, we assume that V_{source}, V_{sky}, V_{load}, and T_{bg} can be measured exactly. We can now calculate the variance of T_A^* with respect to the free variables T_m, T_{load}, T_{spill}, R_i, η_l, τ_s, and τ_i

$$
\begin{aligned}
\sigma^2(T_A^*)^{one-load} \;=\;& \sigma^2(T_m)\left(\frac{\partial T_A^*}{\partial T_m}\right)^2 + \sigma^2(T_{load})\left(\frac{\partial T_A^*}{\partial T_{load}}\right)^2 + \\
& \sigma^2(T_{spill})\left(\frac{\partial T_A^*}{\partial T_{spill}}\right)^2 + \sigma^2(R_i)\left(\frac{\partial T_A^*}{\partial R_i}\right)^2 + \\
& \sigma^2(\eta_l)\left(\frac{\partial T_A^*}{\partial \eta_l}\right)^2 + \sigma^2(\tau_s)\left(\frac{\partial T_A^*}{\partial \tau_s}\right)^2 + \\
& \sigma^2(\tau_i)\left(\frac{\partial T_A^*}{\partial \tau_i}\right)^2 \qquad (35)
\end{aligned}
$$

Calculating the partial derivatives of Equation 19

$$
\begin{aligned}
\frac{\partial T_A^*}{\partial T_m} \;=\;& \gamma\Bigg\{ J'(\nu_s, T_m)\Big[1 - \exp(\tau_s)\Big] + \\
& R_i J'(\nu_i, T_m)\Big[\exp(\tau_s - \tau_i) - \exp(\tau_s)\Big]\Bigg\} \qquad (36) \\
\frac{\partial T_A^*}{\partial T_{load}} \;=\;& \gamma\Bigg\{\Big[J'(\nu_s, T_{load}) + R_i J'(\nu_i, T_{load})\Big]\frac{\exp(\tau_s)}{\eta_l}\Bigg\} \qquad (37) \\
\frac{\partial T_A^*}{\partial T_{spill}} \;=\;& \gamma\Bigg\{ J'(\nu_s, T_{spill})\Big[\exp(\tau_s) - 1\Big] + \\
& \left(1 - \frac{1}{\eta_l}\right) R_i J'(\nu_i, T_{spill}) \exp(\tau_s)\Bigg\} \qquad (38) \\
\frac{\partial T_A^*}{\partial R_i} \;=\;& \gamma\Bigg\{\Big[J(\nu_i, T_{load}) - J(\nu_i, T_{spill})\Big]\frac{\exp(\tau_s)}{\eta_l} + \\
& \Big[J(\nu_i, T_{spill}) - J(\nu_i, T_m)\Big]\exp(\tau_s) + \\
& \Big[J(\nu_i, T_m) - J(\nu_i, T_{bg})\Big]\exp(\tau_s - \tau_i)\Bigg\} \qquad (39)
\end{aligned}
$$

$$
\begin{aligned}
\frac{\partial T_A^*}{\partial \eta_l} &= \gamma \Bigg\{ \Bigg[J(\nu_s, T_{spill}) - J(\nu_s, T_{load}) \\
&\quad + R_i \big[J(\nu_i, T_{spill}) - J(\nu_i, T_{load}) \big] \Bigg] \frac{\exp(\tau_s)}{\eta_l^2} \Bigg\} && (40) \\
\frac{\partial T_A^*}{\partial \tau_s} &= \gamma \Bigg\{ \Bigg[J(\nu_s, T_{load}) - J(\nu_s, T_{spill}) + \\
&\quad R_i \big[J(\nu_i, T_{load}) - J(\nu_i, T_{spill}) \big] \Bigg] \frac{\exp(\tau_s)}{\eta_l} + \\
&\quad \Bigg[J(\nu_s, T_{spill}) - J(\nu_s, T_m) + \\
&\quad R_i \big[J(\nu_i, T_{spill}) - J(\nu_i, T_m) \big] \Bigg] \exp(\tau_s) + \\
&\quad R_i \big[J(\nu_i, T_m) - J(\nu_i, T_{bg}) \big] \exp(\tau_s - \tau_i) \Bigg\} && (41) \\
\frac{\partial T_A^*}{\partial \tau_i} &= \gamma \Bigg\{ R_i \Bigg[J(\nu_i, T_{bg}) - J(\nu_i, T_m) \Bigg] \exp(\tau_s - \tau_i) \Bigg\} && (42)
\end{aligned}
$$

where we have defined

$$
\gamma \equiv \frac{V_{source} - V_{sky}}{V_{load} - V_{sky}} \tag{43}
$$

Substituting the partial derivatives into our variance equation leads to the following equation for the variance of T_A^* in the one-load chopper wheel technique

$$
\begin{aligned}
\sigma^2(T_A^*)^{one-load} \;=\;& \gamma^2 \Bigg\{ \sigma^2(T_m) \Big\{ J'(\nu_s, T_m) \Big[1 - \exp(\tau_s) \Big] + \\
& R_i J'(\nu_i, T_m) \Big[\exp(\tau_s - \tau_i) - \exp(\tau_s) \Big] \Big\}^2 + \\
& \sigma^2(T_{load}) \Big\{ \Big[J'(\nu_s, T_{load}) + R_i J'(\nu_i, T_{load}) \Big] \frac{\exp(\tau_s)}{\eta_l} \Big\}^2 + \\
& \sigma^2(T_{spill}) \Big\{ J'(\nu_s, T_{spill}) \Big[\exp(\tau_s) - 1 \Big] + \\
& \left(1 - \frac{1}{\eta_l}\right) R_i J'(\nu_i, T_{spill}) \exp(\tau_s) \Big\}^2 + \\
& \sigma^2(R_i) \Big\{ \Big[J(\nu_i, T_{load}) - J(\nu_i, T_{spill}) \Big] \frac{\exp(\tau_s)}{\eta_l} + \\
& \Big[J(\nu_i, T_{spill}) - J(\nu_i, T_m) \Big] \exp(\tau_s) + \\
& \Big[J(\nu_i, T_m) - J(\nu_i, T_{bg}) \Big] \exp(\tau_s - \tau_i) \Big\}^2 + \\
& \sigma^2(\eta_l) \Big\{ \Big[J(\nu_s, T_{spill}) - J(\nu_s, T_{load}) + \\
& R_i \big[J(\nu_i, T_{spill}) - J(\nu_i, T_{load}) \big] \Big] \frac{\exp(\tau_s)}{\eta_l^2} \Big\}^2 + \\
& \sigma^2(\tau_s) \Big\{ \Big[J(\nu_s, T_{load}) - J(\nu_s, T_{spill}) + \\
& R_i \big[J(\nu_i, T_{load}) - J(\nu_i, T_{spill}) \big] \Big] \frac{\exp(\tau_s)}{\eta_l} + \\
& \Big[J(\nu_s, T_{spill}) - J(\nu_s, T_m) + \\
& R_i \big[J(\nu_i, T_{spill}) - J(\nu_i, T_m) \big] \Big] \exp(\tau_s) + \\
& R_i \big[J(\nu_i, T_m) - J(\nu_i, T_{bg}) \big] \exp(\tau_s - \tau_i) \Big\}^2 + \\
& \sigma^2(\tau_i) \Big\{ R_i \big[J(\nu_i, T_{bg}) - J(\nu_i, T_m) \big] \exp(\tau_s - \tau_i) \Big\}^2 \Bigg\} \qquad (44)
\end{aligned}
$$

To get an order-of-magnitude estimate of $\sigma^2(T_A^*)$ and $(T_A^*)^2$, we assume $J(\nu,T) \simeq T$, $J'(\nu,T) \simeq 1$, $\eta_l \simeq 1$, $\tau_s \simeq \tau_i$, $T_{load} \simeq T_m \simeq T_{spill} \gg T_{bg}$, $\sigma(T_{load}) \simeq \sigma(T_m) \simeq \sigma(T_{spill})$, and $\sigma(\tau_s) \simeq \sigma(\tau_i)$. Doing this with Equation 44 and the square of Equation 19, we get the following

$$\begin{aligned}
\sigma^2(T_A^*)^{one-load} &= \gamma^2 \Bigg\{ \mathcal{O}\left(\sigma^2(T_m)\Big[\big[1-\exp(\tau_s)\big](1+R_i)\Big]^2\right) + \\
&\quad \mathcal{O}\left(\sigma^2(T_m)\Big[(1+R_i)\exp(\tau_s)\Big]^2\right) + \\
&\quad \mathcal{O}\left(\sigma^2(T_m)\Big[\exp(\tau_s)-1\Big]^2\right) + \\
&\quad \mathcal{O}\left(\sigma^2(R_i)T_m^2\right) + \\
&\quad \mathcal{O}\left(2\sigma^2(\tau_s)\Big[R_i T_m\Big]^2\right)\Bigg\} \qquad (45)\\
\left((T_A^*)^2\right)^{one-load} &= \gamma^2 \Big\{\mathcal{O}(T_m + R_i)\Big\}^2 \qquad (46)
\end{aligned}$$

and we get the following order-of-magnitude relation for $\left(\frac{\sigma(T_A^*)}{T_A^*}\right)^{one-load}$

$$\mathcal{O}\left(\frac{\sigma(T_A^*)}{T_A^*}\right)^{one-load} = \frac{\sqrt{\mathcal{O}\left(\sigma^2(T_m)\Big[1-\exp(\tau_s)+R_i\Big]^2\right) + \mathcal{O}\left(\sigma^2(T_m)\Big[(1+R_i)\exp(\tau_s)\Big]^2\right)}}{\mathcal{O}(T_m+R_i)} \qquad (47)$$

4.4 Comparative Uncertainty of the One- and Two-Load Chopper Wheel Calibration Techniques

In Table 1 we have listed values for each term in the variance relations $\left(\frac{\sigma(T_A^*)}{T_A^*}\right)^{one-load}$ (Equation 44 divided by Equation 19) and $\left(\frac{\sigma(T_A^*)}{T_A^*}\right)^{two-load}$

(Equation 33). For these calculations we assumed

- a zenith atmospheric opacity at each frequency based on atmospheric model calculations assuming 1mm PWV on the Chajnantor site;
- that the elevation of observation was 45°;
- double sideband receiver systems;
- load temperatures and regulation accuracy for the two-load calibration system characteristic of those used in the BIMA prime focus calibration system. In that system, there are two temperature-regulated loads at 310 K and 400 K which couple to the receiver feed with an efficiency of about 2%. The accuracy of the temperature regulation is 0.1% of the measured signal difference.

Four calculations are shown for each frequency, representing (1) best-case conditions, (2) uncertain T_m, (3) uncertain load temperatures, and (4) uncertain atmospheric opacities. Plots of the contributions of each error term to the total uncertainty are shown in Figures 2, 3, and 4. The conclusions from these comparisons are:

1. The most optimistic conditions lead to uncertainties of approximately 0.5% and 1% for the one- and two-load chopper calibration systems, respectively. The 1% uncertainty value is consistent with the results of the BIMA prime focus two-load calibration system (see Welch *et. al.* 2000).

2. At higher frequencies, the uncertainty in the mean atmospheric temperature and the atmospheric opacity dominate the overall uncertainty of the one-load chopper calibration technique. Atmospheric opacity should be measured to an accuracy of at least 1% to obtain <2% overall uncertainty with the two-load calibration system.

3. As the order-of-magnitude relations for $\left(\frac{\sigma(T_A^*)}{T_A^*}\right)^{one-load}$ (Equation 47) and $\left(\frac{\sigma(T_A^*)}{T_A^*}\right)^{two-load}$ (Equation 34) indicate, accurate knowledge of the relative (R_i) and absolute (G_s) sideband gain are important. For example, if $\sigma(R_i) = 10\%$ rather than the standard value of 1%, the best-case uncertainty in the one- and two-load chopper calibration techniques become 5% and 10%, respectively, at 230 GHz.

Table 1: Chopper Wheel Calibration Uncertainty

$\frac{\sigma(T_m)}{T_m}$	$\frac{\sigma(T_{load})}{T_{load}}$	$\frac{\sigma(T_{spill})}{T_{spill}}$	$\frac{\sigma(R_i)}{R_i}$	$\frac{\sigma(\eta_l)}{\eta_l}$	$\frac{\sigma(\tau_s)}{\tau_s}$	$\frac{\sigma(\tau_i)}{\tau_i}$	$\frac{\sigma(T_{load,1})}{T_{load,1}}$	$\frac{\sigma(T_{load,2})}{T_{load,2}}$	$\frac{\sigma(T_A^*)}{T_A^*}^{one-load}$	$\frac{\sigma(T_A^*)}{T_A^*}^{two-load}$ [a]
$\nu = 230$ GHz[b]										
$\frac{10}{268}$	$\frac{0.1}{268}$	$\frac{1}{0.95T_m}$	$\frac{0.01}{1.0}$	$\frac{0.01}{0.98}$	$\frac{0.0007}{0.07}$	$\frac{0.0007}{0.07}$	$\frac{0.001}{6.0}$	$\frac{0.001}{8.0}$	0.6%	1.4%
$\frac{20}{268}$	$\frac{0.1}{268}$	$\frac{1}{0.95T_m}$	$\frac{0.01}{1.0}$	$\frac{0.01}{0.98}$	$\frac{0.0007}{0.07}$	$\frac{0.0007}{0.07}$	$\frac{0.001}{6.0}$	$\frac{0.001}{8.0}$	0.7%	1.4%
$\frac{10}{268}$	$\frac{1.0}{268}$	$\frac{1}{0.95T_m}$	$\frac{0.01}{1.0}$	$\frac{0.01}{0.98}$	$\frac{0.0007}{0.07}$	$\frac{0.0007}{0.07}$	$\frac{0.01}{6.0}$	$\frac{0.01}{8.0}$	0.7%	1.6%
$\frac{10}{268}$	$\frac{0.1}{268}$	$\frac{1}{0.95T_m}$	$\frac{0.01}{1.0}$	$\frac{0.01}{0.98}$	$\frac{0.007}{0.07}$	$\frac{0.007}{0.07}$	$\frac{0.001}{6.0}$	$\frac{0.001}{8.0}$	0.7%	1.6%
$\nu = 490$ GHz										
$\frac{10}{268}$	$\frac{0.1}{268}$	$\frac{1}{0.95T_m}$	$\frac{0.01}{1.0}$	$\frac{0.01}{0.98}$	$\frac{0.01}{1.1}$	$\frac{0.01}{1.1}$	$\frac{0.001}{6.0}$	$\frac{0.001}{8.0}$	7.8%	1.7%
$\frac{20}{268}$	$\frac{0.1}{268}$	$\frac{1}{0.95T_m}$	$\frac{0.01}{1.0}$	$\frac{0.01}{0.98}$	$\frac{0.01}{1.1}$	$\frac{0.01}{1.1}$	$\frac{0.001}{6.0}$	$\frac{0.001}{8.0}$	15.6%	1.7%
$\frac{10}{268}$	$\frac{1.0}{268}$	$\frac{1}{0.95T_m}$	$\frac{0.01}{1.0}$	$\frac{0.01}{0.98}$	$\frac{0.01}{1.1}$	$\frac{0.01}{1.1}$	$\frac{0.01}{6.0}$	$\frac{0.01}{8.0}$	7.8%	1.9%
$\frac{10}{268}$	$\frac{0.1}{268}$	$\frac{1}{0.95T_m}$	$\frac{0.01}{1.0}$	$\frac{0.01}{0.98}$	$\frac{0.1}{1.1}$	$\frac{0.1}{1.1}$	$\frac{0.001}{6.0}$	$\frac{0.001}{8.0}$	10.5%	10.1%
$\nu = 650$ GHz										
$\frac{10}{268}$	$\frac{0.1}{268}$	$\frac{1}{0.95T_m}$	$\frac{0.01}{1.0}$	$\frac{0.01}{0.98}$	$\frac{0.01}{1.1}$	$\frac{0.01}{1.1}$	$\frac{0.001}{6.0}$	$\frac{0.001}{8.0}$	7.9%	1.7%
$\frac{20}{268}$	$\frac{0.1}{268}$	$\frac{1}{0.95T_m}$	$\frac{0.01}{1.0}$	$\frac{0.01}{0.98}$	$\frac{0.01}{1.1}$	$\frac{0.01}{1.1}$	$\frac{0.001}{6.0}$	$\frac{0.001}{8.0}$	15.8%	1.7%
$\frac{10}{268}$	$\frac{1.0}{268}$	$\frac{1}{0.95T_m}$	$\frac{0.01}{1.0}$	$\frac{0.01}{0.98}$	$\frac{0.01}{1.1}$	$\frac{0.01}{1.1}$	$\frac{0.01}{6.0}$	$\frac{0.01}{8.0}$	8.0%	1.9%
$\frac{10}{268}$	$\frac{0.1}{268}$	$\frac{1}{0.95T_m}$	$\frac{0.01}{1.0}$	$\frac{0.01}{0.98}$	$\frac{0.1}{1.1}$	$\frac{0.1}{1.1}$	$\frac{0.001}{6.0}$	$\frac{0.001}{8.0}$	10.6%	10.1%

[a] Assumed $\frac{\sigma(G_s)}{G_s} = \frac{\sigma(R_i)}{R_i}$.

[b] The four sample calculations at each frequency shown represent best, uncertain T_m, uncertain T_{load}, $T_{load,1}$, and $T_{load,2}$, and uncertain τ_s and τ_i.

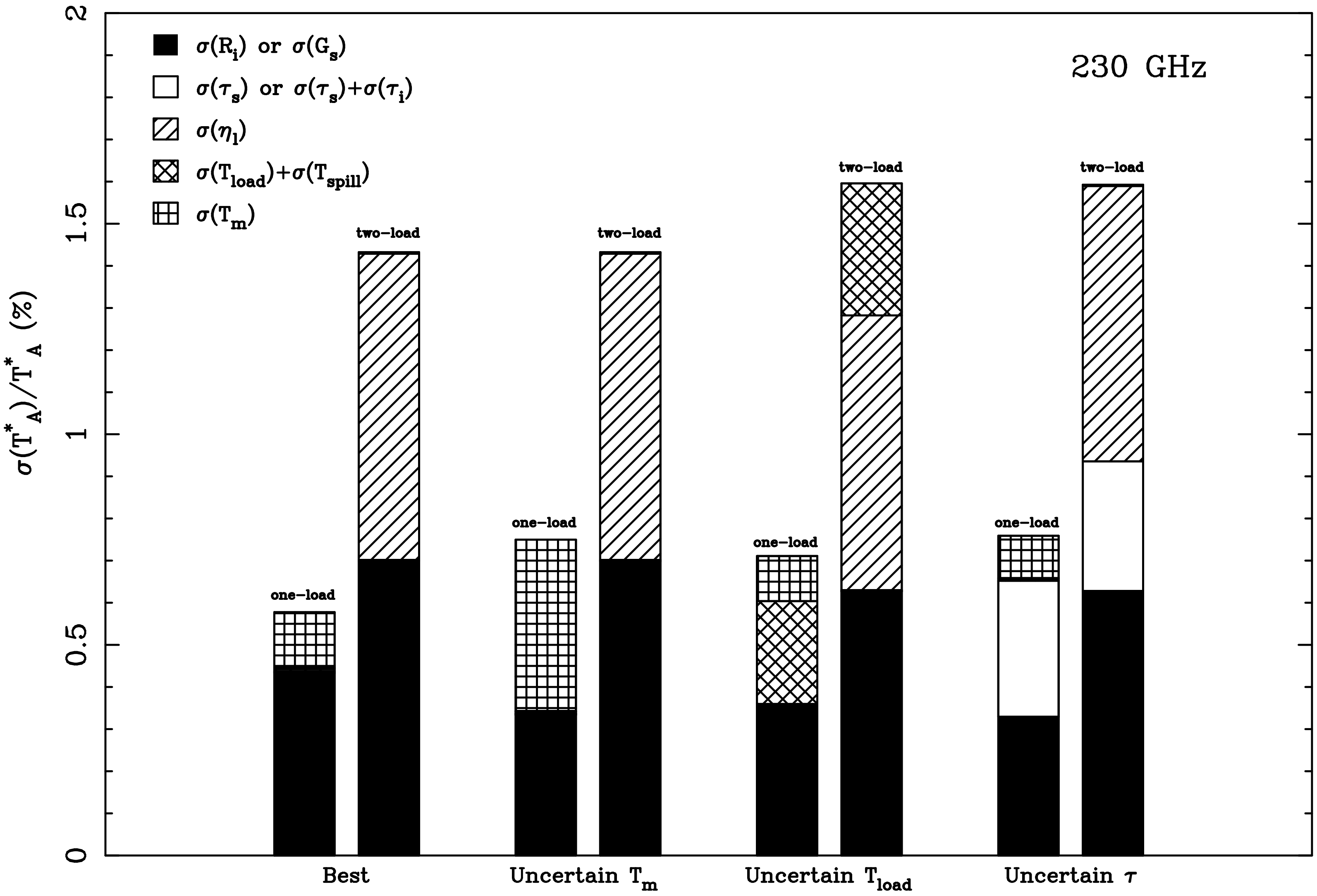

Figure 2: Chopper wheel uncertainties for 230 GHz.

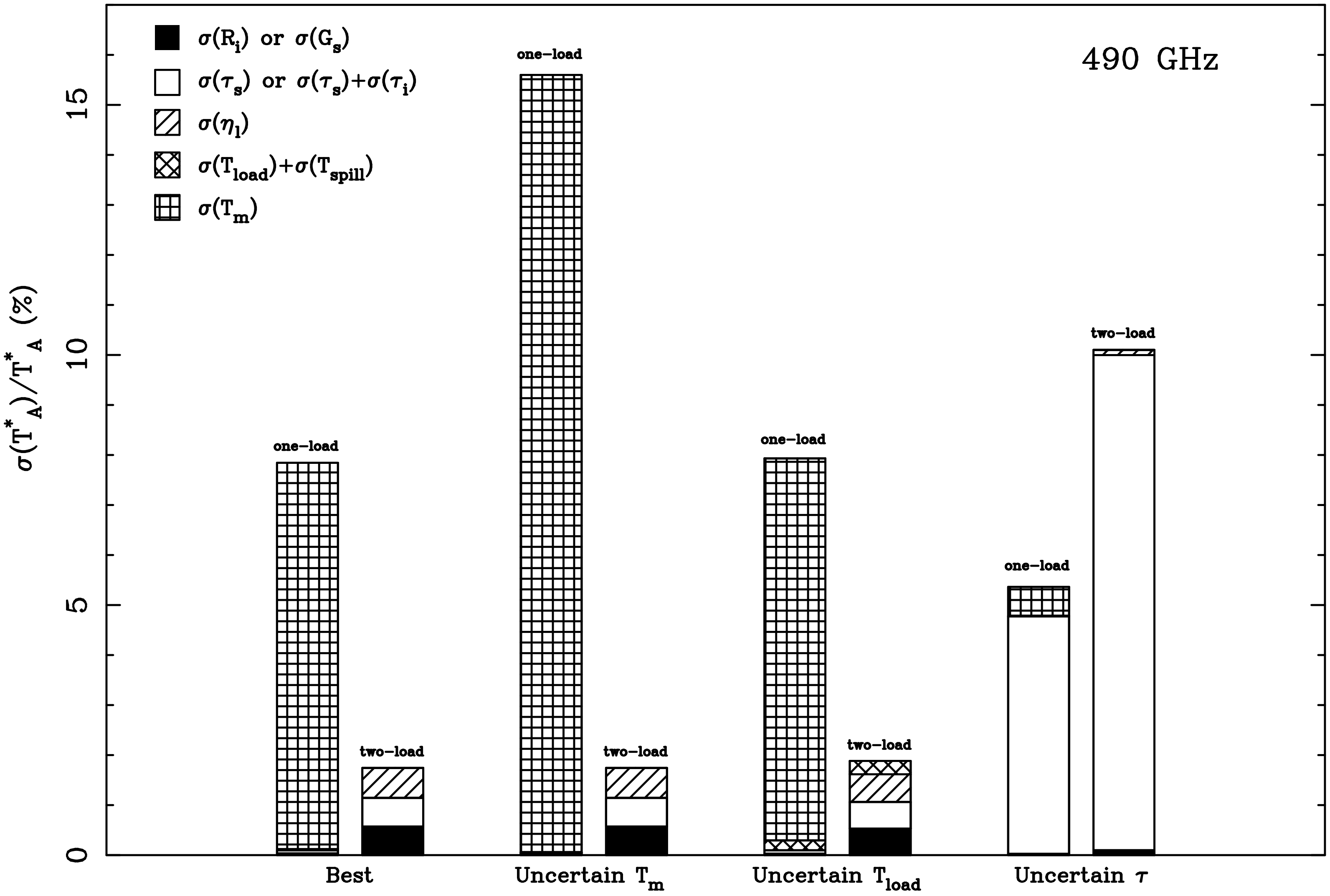

Figure 3: Chopper wheel uncertainties for 490 GHz.

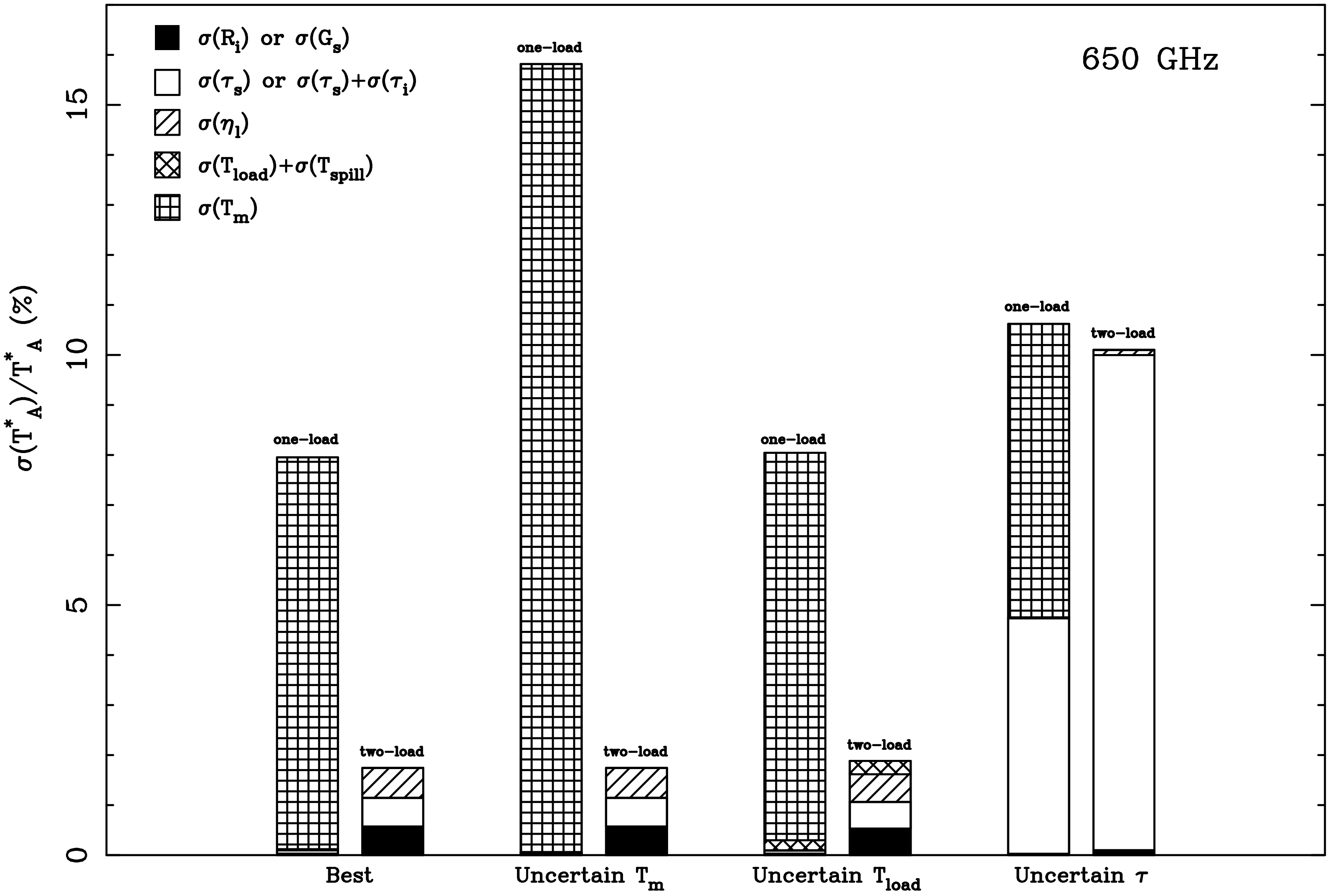

Figure 4: Chopper wheel uncertainties for 650 GHz.

5 The Third Step: Conversion to the $\mathbf{T_R}$ Temperature Scale

This final step in amplitude calibration of single dish and interferometric observations made at millimeter and submillimeter wavelengths relates the telescope-, time-, and position-dependent T_A^* amplitude scale to an astronomical standard. Millimeter and submillimeter single dishes derive the conversion from T_A^* to T_R by measuring planets or satellites with known temperature (see Appendix B for an overview of temperature scales and efficiencies used in millimeter and submillimeter astronomy). The current generation of millimeter and submillimeter interferometers calibrate the amplitudes of their measurements using variants of the following procedure:

1. Measure a planet with "known" amplitude in interferometer mode.

2. Correct planet measurement for resolution affects. This sets the absolute amplitude calibration scale.

3. Measure a quasar in interferometer mode.

4. If you have double sideband receivers, measure the sideband gains on the receivers using a strong source (the quasar from step (3) if it is strong enough, or a planet if it has as much unresolved flux on all baselines as a quasar). The sideband gains are measured in real time and applied to the data, including an additional term for the opacity difference between the two sidebands. This term is model based, scales with elevation angle, and is not significant unless you are near the edge of an atmospheric window. If there is no difference in the opacity between the sidebands, this step can be omitted because any sideband gains will fall out of the calibration. If you have tunerless mixers, then the sideband gains can be assumed to be unity, but the sideband opacity correction should be done in real time if you are near the edge of an atmospheric window.

5. Apply the amplitude calibration scale measured in step 2 to the quasar measurement from step 3. This sets the absolute interferometer amplitude calibration scale. This step need only be done often enough to account for any temporal variations of the quasar flux.

Since ALMA will collect both total power and interferometric measurements, a variant of the calibration procedure suggested by Holdaway (1996) must be used:

1. Measure a standard amplitude calibration source with "known" amplitude using one or all antennas in total power mode to derive the total power amplitude scale.

2. Measure a quasar with one or all antennas in total power mode and absolutely calibrate these measurements using the planet total power measurements from step 1.

3. Measure the same quasar in interferometer mode, applying the amplitude scale derived in step 2 to determine the absolute interferometer amplitude scale. This step need only be done often enough to account for any temporal variations of the quasar flux.

4. If you have double sideband receivers, measure the sideband gains of the receivers using a strong source (the quasar from step (3) if it is strong enough, or a planet if it has as much unresolved flux on all baselines as a quasar). The sideband gains are measured in real time and applied to the data, including an additional term for the opacity difference between the two sidebands. This term is model based, scales with elevation angle, and is not significant unless you are near the edge of an atmospheric window. If there is no difference in the opacity between the sidebands, this step can be omitted because any sideband gains will fall out of the calibration. If you have tunerless mixers, then the sideband gains can be assumed to be unity, but the sideband opacity correction should be done in real time if you are near the edge of an atmospheric window.

In the amplitude calibration procedure listed above, the total power measurement of the standard amplitude calibration source is the most uncertain, representing the last step in the amplitude calibration ladder shown in Figure 1. The difficulty in determining this last step in the amplitude calibration ladder stems from the fact that the requirements for a good astronomical amplitude calibrator:

- Unresolved size;

- Constant or theoretically predictable flux;
- Large amplitude at the frequency of observation.

are met by few if any of the current stable of amplitude calibrators in use at millimeter and submillimeter wavelengths. Table 2 lists the pros and cons associated with traditional (Moon, planets, asteroids, UC HII regions, evolved stars) and proposed (Stars) millimeter and submillimeter amplitude calibrators. Brief descriptions of the millimeter emission properties of each of these types of amplitude calibrator are given in Yun *et. al.* (1998). The amplitude calibrators which hold the most promise for providing the basis upon which an accurate amplitude calibration scale can be derived are asteroids and stars. Evaluation of the millimeter and submillimeter emission properties of these amplitude calibration sources should be one of the very first dedicated research projects conducted on ALMA.

6 Conclusions

1. A two-load chopper wheel calibration system is necessary to have the potential of achieving 1% calibration uncertainty of the T_A^* temperature scale. The main drawback of the two-load calibration system is the need for an independent measurement of the atmospheric opacity τ. This measurement can be derived from a tipping scan or from a dedicated opacity monitor such as a Fourier transform spectrometer system (at each antenna) which monitors the atmospheric opacity continuously at all frequencies.

2. None of the traditional primary flux calibrators satisfy the 1% amplitude calibration requirement specified for ALMA. The derivation of an accurate amplitude calibration scale should be one of the first projects done on ALMA.

Acknowledgments

A very special thanks to Dick Plambeck for reading over several versions of this memo and providing invaluable advice on its content. Thanks also to Steve Scott and Mel Wright for information regarding the amplitude calibration schemes used at OVRO and BIMA, respectively.

Table 2: Primary Amplitude Calibrators at Millimeter and Submillimeter Wavelengths

Source	PRO	CON
Moon	Bright ($T_B \simeq 300K$)	T_B poorly determined Large size and brightness makes it detectable through sidelobes Requires bootstrapping to interferometer flux scale
Planets	Bright ($T_B \simeq 50 - 250K$)	Only Mars has predictable T_B (good to 10-20%) All are extended when observed with the ALMA Planetary atmospheric emission can contaminate flux measurements Requires bootstrapping to interferometer flux scale
Asteroids	Bright ($T_B \simeq 150 - 200K$) Compact ($\theta \simeq 0.2 - 1.3''$) Highly predictable flux Bootstrapping to interferometer flux scale may not be necessary	Oddly shaped Rotation produces flux variation ($\sim$ 4% peak-to-peak in Ceres)
Stars	Compact ($\theta_{\odot} \simeq 1mas$ @ 10pc) Flux predictable with detailed stellar photospheric model Bootstrapping to interferometer flux scale will not be necessary	Presence of dust unknown
UC HII Regions and Evolved Stars	Relatively bright ($T_B \simeq$ few K) Used as secondary flux calibrators at millimeter/submillimeter single dishes	Oddly shaped Sometimes extended Sometimes variable

References

Holdaway, M. A. 1996, MMA Memo 149.

Kutner, M. L. & Ulich, B. L. 1981, ApJ, 250, 341.

Penzias, A. A. & Burrus, C. A. 1973, ARA&A, 11, 51

Ulich, B. L. & Haas, R. W. 1976, ApJS, 30, 247

Yun, M. S., Mangum, J. G., Bastian, T., Holdaway, M., & Welch, W. J. 1998, MMA Memo 211.

Welch, W. J., Bock, D. C.-J., Fleming, M. C., & Thornton, D. D. 2000, in *Imaging at Radio through Submillimeter Wavelengths*

A Definitions

Temperatures

T_{rx} is the receiver DSB noise temperature;

T_{load} is the temperature of the calibration load;

T_m is the mean atmospheric temperature;

T_{spill} is the spillover temperature;

T_{bg} is the cosmic background temperature;

T_{sky}^{cold} is the temperature due to sky emission which terminates to cold sky;

T_{sky}^{hot} is the temperature due to sky emission which terminates to ground;

T_{ant} is the temperature of the antenna;

$T_A(sky)$ is the antenna temperature due to sky emission in the signal or image sideband, respectively;

$T_A(source)$ is the antenna temperature due to source emission;

Other

ν_s is the sky frequency in the signal sideband;

ν_i is the sky frequency in the image sideband;

η_l is the rear spillover, blockage, scattering, and ohmic efficiency;

η_{fss} is the forward spillover efficiency;

τ_s is the atmospheric optical depth in the signal sideband;

τ_i is the atmospheric optical depth in the image sideband;

G_s is the receiver gain in the signal sideband;

G_i is the receiver gain in the image sideband;

$R_i \equiv \frac{G_i}{G_s}$;

K is the proportionality constant between total power voltage and equivalent temperature;

V is the measured voltage from the receiver, which is proportional to the equivalent temperature of the measurement (T) given by the Planck equation;

V_{offset} is the measured DC offset voltage.

Planck Equation: Note that the equivalent Rayleigh-Jeans temperature of the point on the Planck blackbody curve corresponding to the frequency ν, and its derivative with respect to temperature, are given by

$$J(\nu, T) = \frac{\frac{h\nu}{k}}{\exp\left(\frac{h\nu}{kT}\right) - 1} \tag{48}$$

$$\begin{aligned} J'(\nu, T) &= \frac{\partial J(\nu, T)}{\partial T} \\ &= \left(\frac{h\nu}{kT}\right)^2 \frac{\exp\left(\frac{h\nu}{kT}\right)}{\left[\exp\left(\frac{h\nu}{kT}\right) - 1\right]^2} \end{aligned} \tag{49}$$

B Temperature Scales and Telescope Efficiencies

The calibration mode used for essentially all spectral line observations at most millimeter and submillimeter observatories is the chopper wheel method (see Ulich & Haas 1976). The chopper wheel technique corrects for atmospheric attenuation and several telescope losses. In the following, I describe a variety of temperature scales used at many millimeter and submillimeter observatories.

B.1 Definitions

In the following I define the terms used in the subsequent temperature scale and telescope efficiency discussion. I have tried to adopt a similar nomenclature to that used in Kutner & Ulich (1981). Note that throughout this discussion when I refer to a "temperature" I am actually referring to the effective source radiation temperature $J(\nu, T)$, which is defined by Equation 48.

General Terms

$\Omega_s \equiv$ Solid angle subtended by the source

$\Omega_d \equiv$ Solid angle subtended by the central diffraction beam pattern of the telescope

$\Omega \equiv$ Solid angle on the sky

$\Psi \equiv$ Direction angle on the sky

$P_n \equiv$ Normalized antenna power pattern

$P_{ng} \equiv$ Normalized Gaussian antenna power pattern

$B_n \equiv$ Normalized source brightness distribution

$A \equiv$ Airmass toward which the measurement is made

$\tau_0 \equiv$ Atmospheric optical depth at the zenith

$G \equiv$ Maximum antenna gain

Efficiencies

$$
\begin{aligned}
\eta_r &\equiv \text{Radiative efficiency} \\
&\equiv \frac{G}{4\pi}\iint_{4\pi} P_n(\Omega)d\Omega && (50)
\end{aligned}
$$

$$
\begin{aligned}
\eta_{rss} &\equiv \text{Rearward scattering and spillover efficiency} \\
&\equiv \frac{\iint_{2\pi} P_n(\Omega)d\Omega}{\iint_{4\pi} P_n(\Omega)d\Omega} && (51)
\end{aligned}
$$

$$
\eta_l \equiv \eta_r\eta_{rss} \qquad (52)
$$

$$
\begin{aligned}
\eta_{fss} &\equiv \text{Forward scattering and spillover efficiency} \\
&\equiv \frac{\iint_{\Omega_d} P_n(\Omega)d\Omega}{\iint_{2\pi} P_n(\Omega)d\Omega} && (53)
\end{aligned}
$$

$$
\begin{aligned}
\eta_{mb} &\equiv \text{Main beam efficiency} \\
&\equiv \frac{\iint_{4\pi} P_{ng}(\Omega)d\Omega}{\iint_{4\pi} P_n(\Omega)d\Omega} && (54)
\end{aligned}
$$

$$
\begin{aligned}
\eta_{cmb} &\equiv \text{Efficiency at which the source couples to the main diffraction beam} \\
&\quad\ \text{of the telescope} \\
&\equiv \frac{\iint_{\Omega_s} P_n(\Psi-\Omega)B_n(\Psi)d\Psi}{\iint_{4\pi} P_{ng}(\Omega)d\Omega} && (55)
\end{aligned}
$$

$$
\begin{aligned}
\eta_c &\equiv \text{Efficiency at which the source couples to the telescope beam} \\
&\equiv \eta_{cmb}\eta_{mb} \\
&\equiv \frac{\iint_{\Omega_s} P_n(\Psi-\Omega)B_n(\Psi)d\Psi}{\iint_{4\pi} P_n(\Omega)d\Omega} && (56) \\
& && (57)
\end{aligned}
$$

Temperatures

$$T_R \equiv \text{Source radiation temperature}$$

$$\begin{aligned} T_A &\equiv \text{Observed source antenna temperature} \\ &\equiv \frac{GT_R}{4\pi}\exp(-A\tau_0)\iint_{\Omega_s} P_n(\Psi-\Omega)B_n(\Psi)d\Psi \end{aligned} \tag{58}$$

$$\begin{aligned} T'_A &\equiv \text{Observed source antenna temperature corrected for atmospheric attenuation} \\ &\equiv T_A\exp(A\tau_0) \end{aligned} \tag{59}$$

$$\begin{aligned} T^*_A &\equiv \text{Observed source antenna temperature corrected for atmospheric attenuation,} \\ &\quad \text{radiative loss, and rearward scattering and spillover} \\ &\equiv \frac{T'_A}{\eta_r\eta_{rss}} \end{aligned} \tag{60}$$

$$\begin{aligned} T^*_R &\equiv \text{Observed source antenna temperature corrected for atmospheric attenuation,} \\ &\quad \text{radiative loss, and rearward and forward scattering and spillover}^1 \\ &\equiv \frac{T^*_A}{\eta_{fss}} \end{aligned} \tag{61}$$

$$\begin{aligned} \Delta T_R &\equiv \text{Source radiation temperature excluding any background emission} \\ &\quad \text{(like the cosmic microwave background emission)} \\ &\equiv T_R - T_{bg} \\ &\equiv \frac{T^*_R}{\eta_c} \end{aligned} \tag{62}$$

$$\begin{aligned} T_{mb} &\equiv \text{Source brightness temperature as measured by the main diffraction beam} \\ &\quad \text{of the telescope} \\ &\equiv \eta_{cmb}\Delta T_R \end{aligned} \tag{63}$$

[1] T^*_R can also be defined as the source brightness temperature corrected for atmospheric attenuation, radiative loss, and rearward and forward scattering and spillover if the source is equal to or larger than the main diffraction beam.

B.2 Relations Between Temperature Scales

We can now combine the definitions above to derive the relations between the physical measurements and the temperature scales used at many millimeter and submillimeter observatories. Combining the equations above, we can relate the source temperature corrected for atmospheric attenuation (T'_A) to many of the antenna and source temperatures:

$$\begin{aligned} T'_A &= \eta_r \eta_{rss} \eta_{fss} \eta_c \Delta T_R && (64) \\ &= \eta_l \eta_{fss} T^*_R && (65) \\ &= \eta_l T^*_A && (66) \\ &= \eta_{mb} T_{mb} && (67) \end{aligned}$$

B.3 Telescope Efficiency Measurements

Telescope efficiencies are normally calculated using a measurement of the continuum brightness of a planet (for η_{mb}) or the Moon (for η_{fss}). In the following I give the relations used to calculate several telescope efficiencies. Since the source coupling between a disk source like the planets and a Gaussian telescope beam is given by:

$$\eta_{cmb} = 1 - \exp\left[-\ln(2)\left(\frac{\theta_s}{\theta_B}\right)^2\right] \qquad (68)$$

I will use this term in the efficiency equation derivations given below.

B.3.1 Corrected Main Beam Efficiency

The efficiency factor which converts the T^*_A scale to the T_{mb} scale is given by:

$$\begin{aligned} \eta_m &= \frac{T^*_A}{T_{mb}} \\ &= \frac{T^*_A}{(T_R - T_{bg})\left\{1 - \exp\left[-\ln(2)\left(\frac{\theta_s}{\theta_B}\right)^2\right]\right\}} \qquad (69) \end{aligned}$$

One can also calculate η_m using the Ruze equation:

$$\eta_m = \left[1 + \frac{A_e \theta_e^2}{A_m \theta_m^2}\right]^{-1} \tag{70}$$

given that:

$$\begin{aligned}
\theta_e &= 2\sqrt{\ln(2)}\frac{\lambda}{\pi c_\sigma} &(71)\\
\theta_m &= 1.22\frac{\lambda}{D} &(72)\\
\frac{A_e}{A_m} &= \frac{1}{\eta_{a0}}\left[\frac{2c_\sigma}{D}\right]^2 \left\{\exp(\delta^2) - 1\right\} &(73)
\end{aligned}$$

where λ is the wavelength of observation, c_σ is the correlation scale size of the surface deviations, η_{a0} is the zero wavelength aperture efficiency, and δ is the surface accuracy.

B.3.2 Main Beam Efficiency

The efficiency factor which converts any source antenna measurement to the T_{mb} scale is given by:

$$\begin{aligned}
\eta_{mb} &= \frac{T'_A}{T_{mb}}\\
&= \frac{\eta_l T_A^*}{(T_R - T_{bg})\left\{1 - \exp\left[-\ln(2)\left(\frac{\theta_s}{\theta_B}\right)^2\right]\right\}} &(74)
\end{aligned}$$